RSC Advances

PAPER

View Article Online
View Journal | View Issue

Cite this: *RSC Adv.*, 2015, **5**, 32626

The role of H_3PO_4 in the preparation of activated carbon from NaOH-treated rice husk residue

Yaxin Li, Xian Zhang, Ruiguang Yang, Guiying Li and Changwei Hu*

Received 16th March 2015
Accepted 31st March 2015

DOI: 10.1039/c5ra04634c

www.rsc.org/advances

The preparation of activated carbon from rice husk residue using H_3PO_4 as activation agent was studied. The samples were characterized by elemental analysis, N_2 adsorption–desorption, scanning electron microscopy (SEM), X-ray diffraction (XRD), Fourier transform infrared spectroscopy (FT-IR), temperature programmed decomposition-mass spectra (TPD-MS), thermogravimetric analysis (TGA) and X-ray photoelectron spectroscopy (XPS). The role of H_3PO_4 in the activation process was discussed. A maximum surface area of 1016 m^2 g^{-1} was obtained under the optimized conditions, that is, a base treated solid material to H_3PO_4 mass ratio of 1 : 2, an activation temperature of 500 °C and an activation time of 1 h. H_3PO_4 might act as a catalyst which facilitates the release of CO_2, an oxidant which reacts with carbon after dehydration, and a reagent which enters AC through C–O–P bonds.

1. Introduction

Rice is regarded as one of the most important agricultural crops in Asia and the annual quantity of rice husk is very large as a by-product from rice mills. China is the most important rice producer in the world, with an annual output of approximately 200 million tons, whereas most of the rice husk is discarded or directly burned up traditionally.[1] Some researchers have paid attention to the conversion of rice husk into bio-oil,[2,3] and large amount of solid residue named rice husk residue (RHR) is generated at the same time. The utilization of the abundant RHR to produce useful materials is of great significance, not only to avoid the environmental pollution produced from combustion, but also to provide plenty economic benefits.

Activated carbon (AC) is a carbonaceous material with highly developed porosity, and as a result it is generally used as adsorbent, catalyst, and catalyst support.[4] Rice husk from rice mill or rice husk ash after burning from rice husk in paper mill had been used for the production of AC. However, RHR is an interesting potential starting material owing to its low cost. There are only few references reporting its use in AC production.[4–6] The surface area of AC prepared from RHR is usually low because of the high ash content,[7] whereas the ash can be removed by base treatment.

Physical and chemical activation of the starting materials are the two fundamentally employed methods for the preparation of AC. Physical activation involves the carbonization of a precursor using a gaseous activating agent.[8] Chemical activation mixes the precursor with a chemical activating agent, and then heats it in an inert gas. A comparison of chemical activation with physical activation shows that chemical activation needs a lower reaction temperature.[7] Phosphoric acid, zinc chloride and potassium hydroxide are used extensively as activating agents, and there are some differences between them. KOH produces a widening of micropore width, while $ZnCl_2$ develops small mesoporosity, and H_3PO_4 leads to a more heterogeneous pore size distribution.[9] H_3PO_4 has become a common chemical activating agent used for preparing AC from a variety of starting materials,[10–12] because of the lower environmental and toxicological constrains compared to $ZnCl_2$, and lower working temperature compared with KOH or NaOH.[12] As reported before, the best activation temperature was 800 °C for rice husk activated by NaOH[13] and 900 °C for olive husk activated by KOH,[14] and there was a carbonization step before activation process. Additionally, the corrosiveness of the process should also be taken into consideration, especially with strong base as the activator, which exhibits serious corrosion activity toward the reactor. Additionally, the recycled acid could also be used for neutralizing the solution in the base treatment process, producing silica. It is well known that H_3PO_4 appears to function as both an acid catalyst to promote bond cleavage reactions and a reactant in the formation of crosslinks *via* process, such as cyclization and condensation. H_3PO_4 could also combine with organic species in biomass waste to form phosphate and polyphosphate bridges that connect and crosslink polymer fragments.[15] Furthermore, some of these phosphate groups remain on the carbon surface after the washing step.[16] According to Liou *et al.*,[7] the activation process of rice husk is divided into three stage: the organic matter decomposes into the intermediate of smaller molar mass and releases gaseous volatiles in the initial stage of the activation reaction;

Key Laboratory of Green Chemistry and Technology, Ministry of Education, College of Chemistry, Sichuan University, Chengdu, Sichuan, 610064, China. E-mail: gchem@scu.edu.cn; chwehu@mail.sc.cninfo.net; changweihu@scu.edu.cn; Fax: +86-28-85411105; Tel: +86-28-85411105

the intermediate further decomposes to form other volatile species, tar and char, and H_3PO_4 begin to decompose at the same time; in the third stage, the char reacts with P_2O_5, causing the pores to open. However, the study of the function of H_3PO_4 is not as clear as possible.

The aim of the present work is to take advantage of by-product RHR to produce AC and study the function of H_3PO_4 in the activation process.

2. Experimental

2.1. Materials

RHR was produced from rice husk in a fluidized bed reactor, where rice husk was exposed to 475 °C for less than 2 s to get bio-oil for the purpose of energy material.[17] Sodium hydroxide (NaOH) and phosphoric acid (H_3PO_4, 85%) were of analytical grade and applied without further purification. N_2 was of chemical grade (at a purity of 99.9%). Deionized water was employed throughout all the treatment processes.

2.2. Preparation of activated carbon

RHR (40–80 mesh) was washed with deionized water to remove the impurities, and then dried in an oven at 100 °C for 24 h. 30 g of dried rice husk residue was put into a flask, and 200 mL of 3 mol L^{-1} NaOH solution[18] was added into the reactor, then the temperature was increased to 105 °C and kept for 5 h. NaOH reacted with silica to form soluble Na_2SiO_3. The suspension was filtrated and the base treated solid residue (abbreviated as BTRHR) was washed with deionized water, and then dried for use in the preparation of AC.

2 g of BTRHR was impregnated with 15 mL H_3PO_4 aqueous solution at various BTRHR/H_3PO_4 ratios (1 : 0.5, 1 : 1, 1 : 2, 1 : 2.5 and 1 : 3). The impregnated residue was set into an oven at 100 °C for one night to remove the excess water, and then the dried sample (PBTRHR) was used for activation where it was heated from room temperature at 5 °C min^{-1} up to various activation temperature for different activation time under N_2 flow of 60 mL min^{-1} in a horizontal cylindrical furnace. The resultant sample was washed with deionized water until neutral and dried to obtain AC. The washing water was collected for neutralizing the filtrate of the first step, producing silica. The obtained AC samples were named according to the preparation condition, for example, AC (1 : 2/1/500) meant that the sample was obtained with BTRHR/H_3PO_4 mass ratio of 1 : 2, an activation time of 1 h and an activation temperature of 500 °C.

2.3. Characterization

2.3.1. Elemental analysis. An elemental analyzer (Italy, CARLO ERBA 1106) was used to identify the hydrogen, carbon and nitrogen content of the samples.

2.3.2. N_2 adsorption–desorption. The specific surface area and pore size of AC samples were measured at −196 °C by means of a standard Brunauer–Emmett–Teller (BET) N_2 adsorption procedure (Micromeritics TriStar 3020). The BET surface area (S_{BET}) was based on the BET equation and was calculated using the volume of N_2 adsorbed at relative pressures of 0.01–0.1. The total pore volume was estimated at a relative pressure of 0.995. The *t*-plot method was used to calculate the micropore volume (V_{mic}) and the mesopore volume (V_{mes}) was determined by subtracting the micropore volume from the total pore volume. Pore size distributions were calculated from nitrogen adsorption results using the DFT Plus Software.

2.3.3. Scanning electron microscopy (SEM). The surface morphology of the samples was observed by scanning electron microscopy (SEM, FEI Inspect F) with an acceleration voltage of 20 kV. The sample was gold coated prior to SEM observation.

2.3.4. X-ray diffraction (XRD). The crystalline structure of the samples was obtained using a DX-1000 CSC diffraction instrument at 40 kV and 25 mA. The scanning scope and scanning speed was 5–80° and 0.06° min^{-1}, respectively, using Cu Kα radiation.

2.3.5. Fourier transform infrared spectroscopy (FT-IR) studies. The samples were analyzed by FT-IR on a Nicolet Nexus 670 instrument in order to identify the surface functional groups of the RHR, BTRHR and AC (1 : 2/1/500). They were recorded in the region of 4000–400 cm^{-1} employing the KBr pellet method.

2.3.6. Temperature programmed decomposition. In order to study the reactions occurring during the activation process, temperature programmed decomposition was carried out, and the evolved gases were monitored by a multichannel HP R-20QIC mass spectrometry (TPD-MS). Helium was chosen as carrier gas to avoid the interference between carbon monoxide and nitrogen. The PBTRHR (BTRHR/H_3PO_4 = 1 : 2) was put in a stainless steel Utube. Pure He sweeping was performed at room temperature until the baseline of MS signals stabilized. TPD-MS was conducted from 30 to 800 °C at a ramping of 5 °C min^{-1} under He flow rate of 30 mL min^{-1}. The possible molecules (CO_2, PH_3, O_2, CO and H_2O) released were monitored with MS signals of m/z = 44, 34, 28, and 18. BTRHR was taken out as a reference.

2.3.7. Thermo gravimetric analysis (TGA). A thermo gravimetric analyzer (NETZSCH TGA 209F1) was employed to have a better understanding of the reaction between BTRHR and H_3PO_4. Samples (BTRHR and PBTRHR) were heated to 800 °C at a ramp of 5 °C min^{-1} in N_2 atmosphere. Then, RHR, BTRHR and AC (1 : 2/1/500) were also heated to 800 °C at a ramp of 5 °C min^{-1} in air to get an insight of the change after base treatment and acid activation.

2.3.8. X-ray photoelectron spectroscopy (XPS). XPS was used to provide information on the surface composition of the samples. XPS experiments were performed on an AXIS Ultra DLD (KRATOS) using Al Kα radiation (1486.6 eV), the source being operated at 12 kV and 12 mA. The linear background was subtracted from all spectra. The software XPSPEAK41 was employed to deconvolve the XPS peaks.

3. Results and discussion

3.1. Characterization of the samples

3.1.1. Elemental analysis and N_2 adsorption–desorption. The results of elemental analysis and N_2 adsorption–desorption of RHR, BTRHR and AC (1 : 2/1/500) were shown in Table 1. The

Table 1 Elemental analysis and N_2 adsorption–desorption of RHR, BTRHR and AC (1 : 2/1/500)

Sample name	RHR	BTRHR	AC (1 : 2/1/500)
Elemental composition (wt%)			
C	42.00	67.20	70.62
H	2.08	3.09	2.09
N	0.34	0.65	0.56
N_2 adsorption–desorption			
S_{BET} (m^2 g^{-1})	96	201	1016
V_t (cm^3 g^{-1})	0.059	0.13	0.53
V_{mic} (cm^3 g^{-1})	0.031	0.055	0.31
V_{mes} (cm^3 g^{-1})	0.028	0.075	0.22

relative percentage of carbon, hydrogen and nitrogen elements increased after base treatment because of the removal of silica. Then, the percentage of carbon element was increased after activation process. However, hydrogen and nitrogen elements followed the opposite variation trend. The decrease in hydrogen and nitrogen may be attributed to the formation of vapor, ammonia or other substance. Similar results were reported by Liou *et al.*[7] The rest components of the samples were oxygen and ash.

According to N_2 adsorption–desorption results, the surface area, the total pore volume, microporous volume and the mesoporous volume increased dramatically after base treatment and activation process. It could be concluded that a porous structure was leaving behind after the removal of silica. Moreover, H_3PO_4 activation process made more porous structure.

3.1.2. SEM. Fig. 1 presented the SEM pictures of RHR, BRRHR, and AC (1 : 2/1/500) with different magnifications. From Fig. 1a–c the corrugated epidermis could be observed, and there is no noticeable difference between RHR and rice husk. New pores formed with the release of silica by the base treatment according to Fig. 1d–f. The pictures of AC (1 : 2/1/500) was shown in Fig. 1g–i.

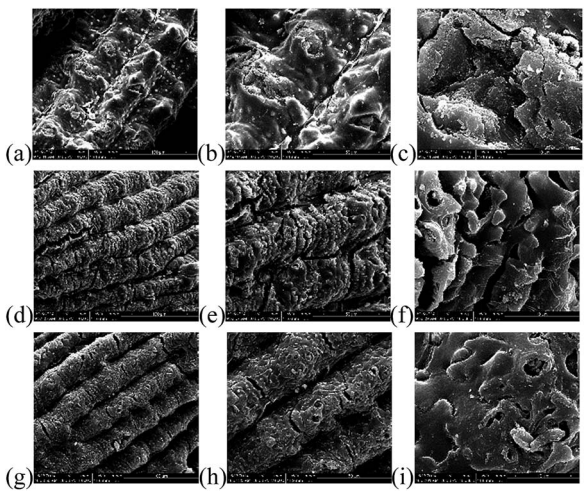

Fig. 1 SEM of (a–c) RHR, (d–f) BTRHR and (g–i) AC (1 : 2/1/500) with different magnifications.

3.1.3. XRD. The X-ray spectra of RHR, BTRHR and AC (1 : 2/1/500) were shown in Fig. 2. Fig. 2a showed a characteristic peak of silica, which corresponded to the presence of cristobalite in ash.[1] After base treatment and H_3PO_4 activation, BTRHR and AC (1 : 2/1/500) showed two vital peaks at 25 and 42°, indicating the existence of the (002) and (100) planes, of the graphitic structure, respectively.[19,20]

3.1.4. FT-IR. Fig. 3 displayed the FT-IR results. From 4000 to 1400 cm^{-1}, the samples showed no distinct change. Four bonds in this range were observed. The wide band located around 3400 cm^{-1} was attributed to ν(O–H) vibration in hydroxyl groups or adsorbed water.[21] The small band at 2920 cm^{-1} was ν(C–H) stretching vibration of $-CH_2$.[22] The band near 1600 cm^{-1} was due to aromatic ring or ν(C=C) vibration and the band around 1400 cm^{-1} could be assigned to ν(C–O) vibration in the carboxylate group.[23] From 1400 to 400 cm^{-1}, there were some differences between the samples. RHR had three bands around 1090, 798 and 460 cm^{-1}. The results were probably caused by the silicon atom initially attached to the oxygen atom.[24] However, BTRHR didn't have these bands, indicating the removal of silica.

The adsorption around 1180 cm^{-1} of AC (1 : 2/1/500) might be assigned to the stretching mode of hydrogen-bonded P=O, to O–C stretching vibrations in P–O–C (aromatic) linkage and to P=OOH.[25]

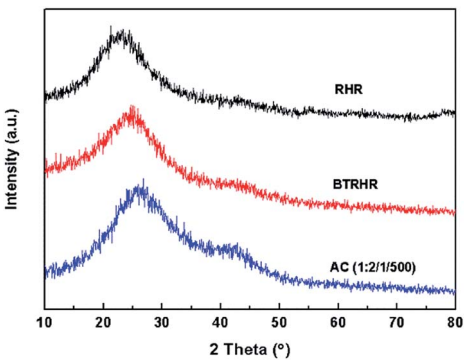

Fig. 2 XRD of RHR, BTRHR and AC (1 : 2/1/500).

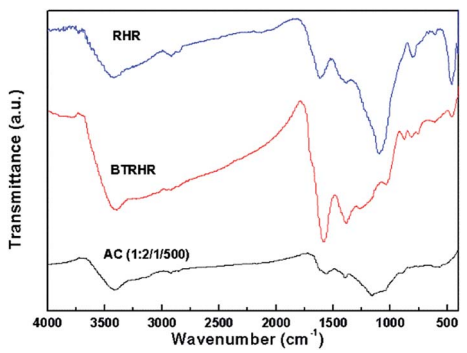

Fig. 3 FT-IR spectrogram of samples: RHR, BTRHR and AC (1 : 2/1/500).

3.2. Optimization of preparation conditions

3.2.1. Effect of activation temperature. The effect of activation temperature on the surface area and pore volume of phosphoric acid treated BTRHR was investigated at BTRHR/H_3PO_4 ratio of 1 : 2 with activation time of 1 h. As shown in Table 2, the activation temperature exhibited significant influence on the textural properties. The surface area and pore volume gradually increased with activation temperature from 300 to 500 °C. At 500 °C, the sample showed remarkably improved porosity compared with the samples activated at other activation temperature, with a maximum surface area and total pore volume of 1016 $m^2\ g^{-1}$ and 0.53 $cm^3\ g^{-1}$, respectively. However, the surface area and pore volume decreased with further increase in temperature from 500 to 700 °C.

At low activation temperature of 300 and 400 °C, the pore structure might not fully develop.[7] However, when the temperature was higher than 500 °C, violent gasification reactions might cause part of the micropore structure to be destroyed by collapsing or combining together.[26]

Fig. 4a showed the N_2 adsorption–desorption isotherms of AC prepared at different temperature. According to the IUPAC classification,[27] these isotherms seemed to be Type I, which means AC was microporous. When the relative pressure increased above 0.4, the isotherms showed hysteresis loops which were the Type H4 loop. The DFT pore size distributions of AC prepared at different temperature were shown in Fig. 4b. The sample produced at activation temperature of 500 °C showed the strongest pore width at 10 Å. It could be concluded that 500 °C was the optimum activation temperature. The best activation temperature of 500 °C was reported for AC preparation from different waste such as grape seeds,[12] rice husk[26] and bituminous coal.[28] Other optimized activation temperature for AC production from rice hull[21] and rice husk[19] at 400 and 900 °C were also reported. The material of this study was the residue of rice husk which had been used in bio-oil production. Although it was different from these original wastes, the best activation temperature was still 500 °C.

3.2.2. Effect of BTRHR/H_3PO_4 ratio. It is well known that the BTRHR/H_3PO_4 ratio was one of the variables having significant influence on the porosity of the AC obtained.[29] Table 3 showed the textural parameters of AC prepared at different BTRHR/H_3PO_4 ratios activated at 500 °C for 1 h. When the BTRHR/H_3PO_4 ratio was increased from 1 : 1 to 1 : 3, the surface area of AC increased from 553 $m^2\ g^{-1}$ at a ratio of 1 : 1 and reached a maximum of 1016 $m^2\ g^{-1}$ at a ratio of 1 : 2, and then decreased. The total pore volume, microporous volume and the mesoporous volume followed the same tendency as the surface area.

The inadequate development of porous structure was observed at the BTRHR/H_3PO_4 ratio of 1 : 1 and 1 : 1.5. This might be due to the insufficient amount of phosphoric acid, which could not activate the sample effectively. However, when the BTRHR/H_3PO_4 ratio was higher than 1 : 2, the surface area and pore volume decreased. This observation was probably due to the phosphate and polyphosphate species which are incorporated into the carbon matrix through C–O–P bonds.[30] Part of the porosity of AC was blocked by phosphorus compounds, which are not easily removed with washing.[7]

N_2 adsorption–desorption isotherms and pore size distributions of the samples activated at different BTRHR/H_3PO_4 ratios were shown in Fig. 4c and d. All the samples displayed Type I isotherms and H4 hysteresis loop. The sample produced at a BTRHR/H_3PO_4 ratio of 1 : 2 showed the strongest pore width at 10 Å compared with other BTRHR/H_3PO_4 ratio. It could be concluded that an appropriate BTRHR/H_3PO_4 ratio was beneficial to the formation of the pore structure. Consequently, keeping the BTRHR/H_3PO_4 ratio at 1 : 2 could lead to a favorable development of the porosity in AC. Other rice husk to phosphoric acid ratios such as 1 : 2 (85% of phosphoric acid),[7] 1 : 5 (50% of phosphoric acid),[31] and 1 : 4.2 (100% of phosphoric acid)[19] were reported. Additionally, jackfruit peel waste to phosphoric acid ratio and waste tires to phosphoric acid ratio of 1 : 4 (85% of phosphoric acid)[32] and 1 : 5 (100% of phosphoric acid)[33] were reported, respectively. The BTRHR/H_3PO_4 mass ratio of 1 : 2 (85% of phosphoric acid) in our study was lower than or equal to the value in reported studies.

3.2.3. Effect of activation time. The effect of activation time on the surface area and pore volume of AC were investigated at the activation temperature of 500 °C and the BTRHR/H_3PO_4 ratio of 1 : 2. As shown in Table 4, the textural properties increased from 1007 $m^2\ g^{-1}$ for 0.75 h and reached a maximum of 1016 $m^2\ g^{-1}$ for 1 h, and then decreased. When activated for 0.75 h, the pore structure was inadequately developed and had inferior textural properties, denoting incomplete reaction between BTRHR and H_3PO_4. When activated for 1 h, the sample exhibited the best pore structure development, indicating that this activation time enabled sufficient reaction. However, when activated for 1.5 and 2 h, the surface area and porosity decreased because the excessive reaction damaged the pores that had already formed. Fig. 4e and f displayed the adsorption–desorption isotherms and DFT pore size distributions of AC. It could be concluded that the activation time of 1 h can be considered as a suitable point. Similar behavior (activated for

Table 2 Textural properties of AC prepared at different temperature on the BTRHR/H_3PO_4 ratio of 1 : 2 and the activation time of 1 h

Activation temperature (°C)	S_{BET} ($m^2\ g^{-1}$)	V_t ($cm^3\ g^{-1}$)	V_{mic} ($cm^3\ g^{-1}$)	V_{mes} ($cm^3\ g^{-1}$)
300	633	0.33	0.19	0.14
400	910	0.47	0.28	0.19
500	1016	0.53	0.31	0.22
600	996	0.50	0.31	0.19
700	651	0.32	0.21	0.11

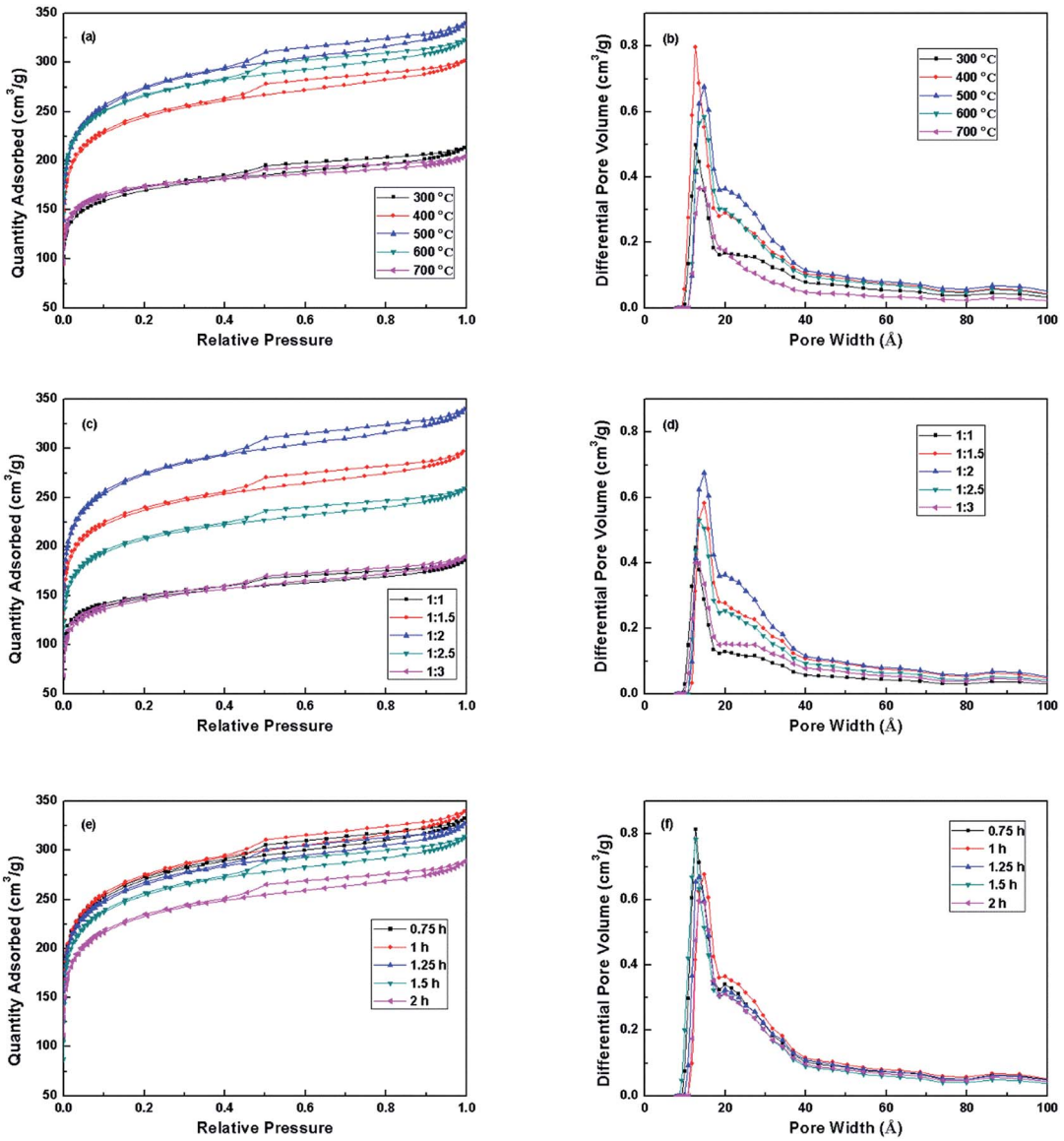

Fig. 4 N_2 adsorption–desorption isotherms and DFT pore size distributions for AC with different activation temperature (a and b), different impregnation ratios (c and d) and different activation time (e and f).

Table 3 Textural properties of AC prepared at different BTRHR/H_3PO_4 ratio on the activation temperature of 500 °C and the activation time of 1 h

BTRHR/H_3PO_4 ratio	S_{BET} ($m^2\ g^{-1}$)	V_t ($cm^3\ g^{-1}$)	V_{mic} ($cm^3\ g^{-1}$)	V_{mes} ($cm^3\ g^{-1}$)
1 : 1	553	0.29	0.17	0.12
1 : 1.5	886	0.46	0.27	0.19
1 : 2	1016	0.53	0.31	0.22
1 : 2.5	773	0.40	0.23	0.17
1 : 3	543	0.29	0.16	0.13

1 h) was observed for the materials of rice husk and corncob.[10,26,34] Other materials such as rice straw,[11] hemp stem and olive stones[16] needed 2 h activation to prepare AC.

Overall, an activation temperature of 500 °C, a BTRHR/H_3PO_4 ratio of 1 : 2 and an activation time of 1 h were selected as the most adaptable condition for the preparation of AC.

3.3. The role of H_3PO_4 in the activation process

3.3.1. TPD-MS and TGA-DTG. Fig. 5 showed the CO_2, CO, H_2O and PH_3 TPD-MS spectra of BTRHR and PBTRHR. The CO_2 spectra of BTRHR showed two emission peaks. The first covered the range between 150 and 590 °C with a maximum at 430 °C, which was associated with the decomposition of carboxylic

Table 4 Textural properties of AC prepared at different activation time on the activation temperature of 500 °C and the BTRHR/H_3PO_4 ratio of 1 : 2

Activation time (h)	S_{BET} ($m^2\ g^{-1}$)	V_t ($cm^3\ g^{-1}$)	V_{mic} ($cm^3\ g^{-1}$)	V_{mes} ($cm^3\ g^{-1}$)
0.75	1007	0.51	0.31	0.20
1	1016	0.53	0.31	0.22
1.25	987	0.51	0.30	0.21
1.5	947	0.49	0.29	0.20
2	865	0.45	0.26	0.19

acids below 240 °C, lactones and carboxylic anhydrides at higher temperature.[12] Another emission peak was attributed to reaction of phenols and carbonyls with a maximum at 710 °C from 590 to 800 °C. In the stage of constant temperature, it displayed a downward trend. The CO_2 spectra of PBTRHR showed also two peaks of emission. The first covered the range between 100 and 650 °C with a maximum located at 360 °C. At higher temperature (>650 °C), the spectra showed the beginning of a new step, maximized at 800 °C and then decreased at the constant temperature stage. From the decomposition spectra of CO_2, it would be known that at lower temperature H_3PO_4 might act as a catalyst, facilitating the release of CO_2; and at higher temperature H_3PO_4 might react with BTRHR, generating more CO_2.

A gently increase of CO could be seen from the spectra of BTRHR from 110 to 800 °C and then decreased in the constant stage. This could be assigned to the decomposition of carbonyl, quinone and/or ether oxygenated species.[35] A gently increase of CO desorption of PBTRHR took place from 110 to 700 °C and then a sharp increase of CO could be seen from the spectra of PBTRHR above 700 °C. During the constant stage the spectra decreased as well. According to the CO spectra of the samples, some reactions might exist above 700 °C for PBTRHR.

Fig. 5 showed the evolution of H_2O. BTRHR exhibited a peak at about 105 °C, ascribed to desorption of adsorbed water. At higher temperature, BTRHR displayed a low and continuous release of H_2O with a gentle peak. PBTRHR showed three peaks developed with maxima at 105 and 170 °C below 400 °C, and another peak with maxima at 530 °C between 400 and 800 °C. These peaks should be due to the dehydration of H_3PO_4.

PH_3 spectra of BTRHR showed no PH_3 produced in the process, while, the formation of PH_3 could be seen at higher temperature (>700 °C) for PBTRHR. The peak increased from 700 to 800 °C and then decreased during the constant stage, indicating reductive reaction occurred. The process made the valence state of phosphorus reduced from +5 to −3.

The TGA results of BTRHR and PBTRHR were illustrated in Fig. 6. From 100 to 400 °C, the mass loss of 7.7% for BTRHR and the mass loss of 16.4% for PBTRHR mainly corresponded to the release of H_2O, CO_2 and a small amount of CO. In the temperature range of 400–700 °C and 700–800 °C, the mass loss of 14.8% and 3.9% of BTRHR was attributed to the release of H_2O, CO_2 and CO. The mass loss of PBTRHR at 400–700 °C corresponded to the activation process, in which the mass loss of 30.4% might be attributed to the reaction between the activating agent and carbonaceous residue,[7] producing H_2O, CO_2 and CO. From 700 to 800 °C, the mass loss of 7.6% should be due to the release of CO_2, CO and PH_3.

Fig. 7 showed the TGA (a) and DTG (b) curves of RHR, BTRHR and AC (1 : 2/1/500) in air flow. The mass loss of RHR and BTRHR occurred in the range from 250 to 650 °C, whereas the mass loss of AC occurred in the range from 400 to 800 °C. This indicated that the base treatment did not change the oxidation performance of the samples obviously according to Fig. 7b. However, H_3PO_4 activation process changed the oxidation performance. The peak oxidation temperature increased from 423 °C for BTRHR to 560 °C for AC (1 : 2/1/500). It could be due to the fact that the more highly cross-linked structure was developed after activated by H_3PO_4, which was less prone to volatile loss.[28]

Besides, the ash content decreased after the base treatment compared with RHR because of the ash removal of silica. However, the ash content was increased after activated by H_3PO_4 compared to BTRHR. The reason of the high ash content of AC (1 : 2/1/500) might be linked to the mechanism of H_3PO_4 activation. Phosphoric acid might combine with organic species to form phosphoric linkages, such as phosphate and polyphosphate esters, that result in broader porous structures in AC.[15] Moreover, the incorporated phase contained not only phosphoric acid but a mixture of polyphosphoric acids, including predominant species such as H_3PO_4, $H_4P_2O_7$ and $H_5P_3O_{10}$ and some others in lower proportion (*e.g.* $H_{n+2}P_nO_{3n+1}$) after activation process.[28] The acids could be collected through washing for further use. However, some of these phosphate groups remain on the carbon surface after the washing step, as reported in previous study.[16] Consequently, the ash content was increased after being activated by H_3PO_4.

3.3.2. XPS. Fig. 8 showed the P 2p spectra of PBTRHR and the samples activated by H_3PO_4 at 300, 400, 500, 600, 700 °C. Peaks in the range 134.0–134.6 eV are commonly assigned to phosphate species in which P atom is bonded to O atoms.[36] From XPS, it suggests that P is mainly present on the carbon surface by bonding to O atoms, which is in agreement with the FT-IR observations. However, the distinctions between P 2p spectra of the samples were small, so the O 1s spectra were also discussed.

The O 1s spectra of PBTRHR and the samples activated by H_3PO_4 at 300, 400, 500, 600, 700 °C was shown in Fig. 9. A satisfactory fit was achieved by means of four components: C═O groups and non-bridging oxygen in the phosphate group (P═O) bonds (peak 1, 531.5 eV); singly bonded oxygen (–O–) in C–OH, C–O–C and/or C–O–P (peak 2, 531.9–532.3 eV); P–O–P bonds (peak 3, 533.2 eV); chemisorbed oxygen and water (peak 4, 532.7–533.9 eV).[37–39] According to Table 5, the relative content of peak 1 was reduced with the increase of activation temperature, especially from 500 to 700 °C. The reduction of the relative content of peak 1 might have correlation with the release of CO_2 and/or CO with the increase of temperature and the reductive reaction between phosphorus compounds and BTRHR. The relative content of peak 3 was increased as the temperature rose. The dehydration of phosphoric acid and the change of the structure of phosphorus complexes should be the reason of the

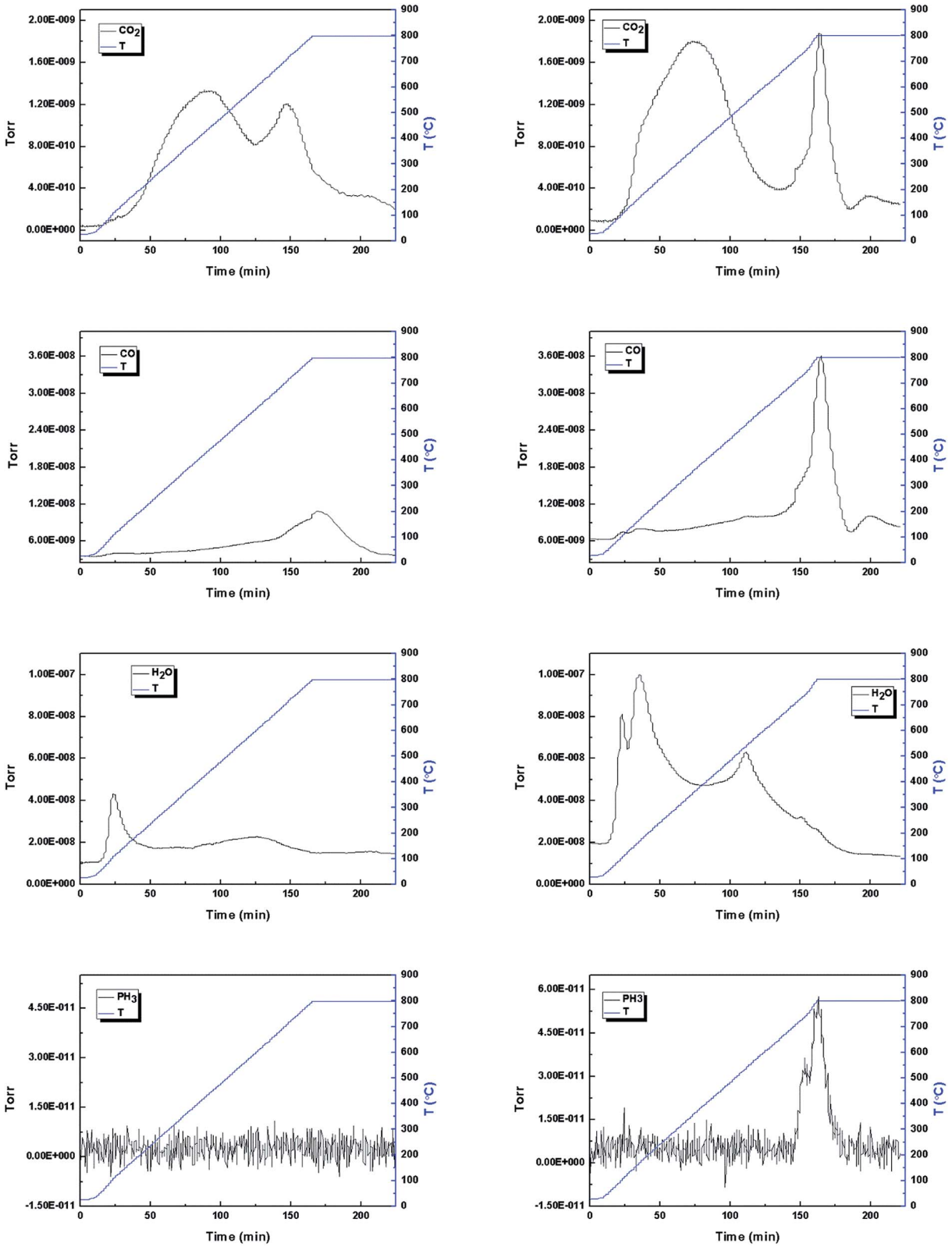

Fig. 5 CO_2, CO, H_2O and PH_3 TPD-MS spectra of BTRHR (left) and PBTRHR (right).

variation of relative content of peak 3. The relative content of peak 2 decreased firstly and reached a minimum of 15.4%, and increased subsequently. Three reasons might affect the variation of the relative content of peak 2: first, the phosphorous compound linked with BTRHR through C–O–P bond; second, the release of CO; third, the phosphorus complexes react with

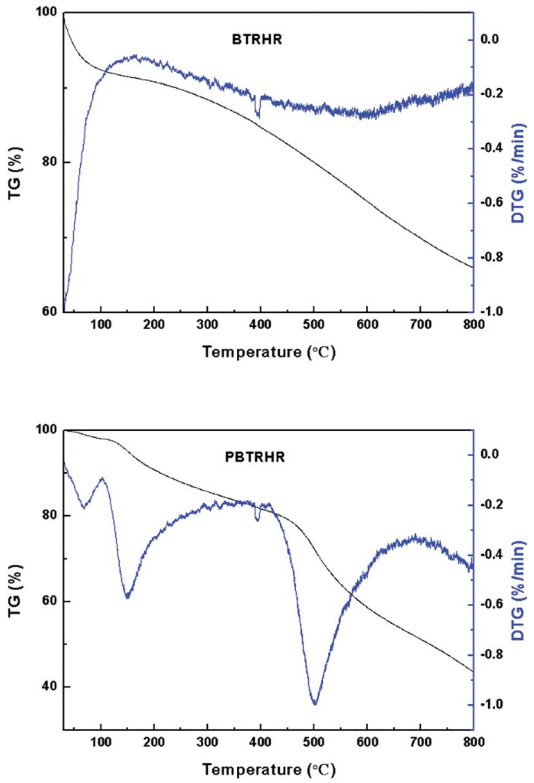

Fig. 6 TGA and DTG curves of BTRHR and PBTRHR.

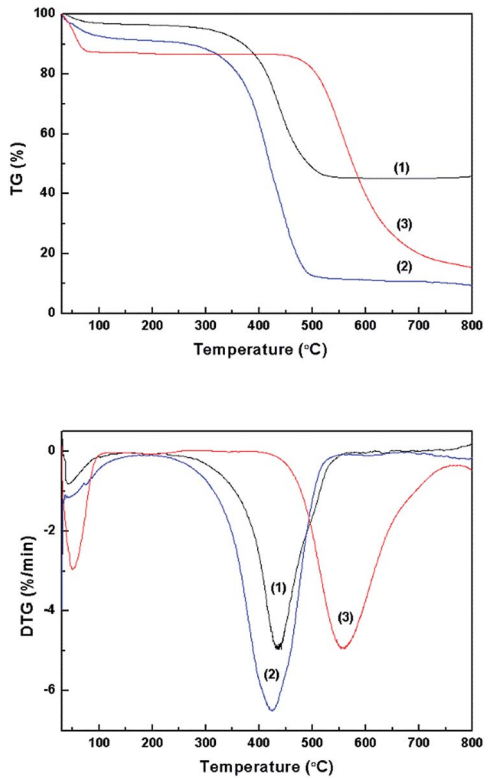

Fig. 7 TGA (a) and DTG (b) curves of (1) RHR, (2) BTRHR and (3) AC (1 : 2/1/500).

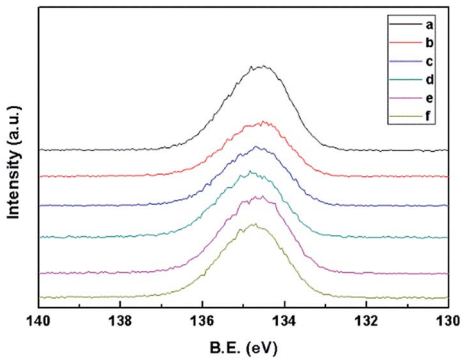

Fig. 8 XPS spectra of P 2p peak of (a) PBTRHR and the samples (b–f) activated at 300, 400, 500, 600 and 700 °C.

other adjacent groups, forming P_4O_{10} and polyphosphates groups.[16,40] Furthermore, the extra water washing after activation might cause reaction between phosphorus residue and water, and thus influence the content of peak 2 and 3. For example, P_4O_6 will react with H_2O to form phosphorous acid again and dissolved during washing.

3.4. Discussion

According to TPD-MS, TGA-DTG, XPS and the structure of phosphorous compound, main reactions which might take place over different temperature range can be supposed as the following.

From 100 to 400 °C, the following reactions might occur:

$$2H_3PO_4 \rightarrow H_4P_2O_7 + H_2O \quad (1)$$

$$3H_3PO_4 \rightarrow H_5P_3O_{10} + 2H_2O \quad (2)$$

$$nH_3PO_4 \rightarrow H_{n+2}P_nO_{3n+1} + (n-1)H_2O \quad (3)$$

The structure of phosphorous compound varied with the increase of temperature, as shown in the H_2O spectra of TPD-MS and the O 1s of XPS. Two peaks and the continuously release of H_2O were shown in the H_2O spectra below 400 °C. It was the dehydration of H_3PO_4, as shown in the reaction (1)–(3). As a result, the content of peak 3 (P–O–P) was increased rapidly from (a) PBTRHR to (c) the sample activated at 400 °C according to Table 5. Furthermore, H_3PO_4 might act as a catalyst, making the release of CO_2 at lower temperature. The content of peak 1 (C=O, P=O) decreased slightly, which might be due to the production of CO_2 decomposed from C=O group. Furthermore, the release of a little amount of CO decomposed from functional groups might decrease the content of peak 1 as well. M. A. Nahil and P. T. Williams suggested that in the range of 150–400 °C the pyrolysis of organic matter in the cotton stalks and dehydration of phosphoric acid were shown in the thermal degradation.[41] BTRHR in our study was different from the original biomass waste because of the bio-oil extraction from rice husk and then the base treatment. Therefore, the composition might have already changed, and the weight loss should be mainly attributed to the dehydration of phosphoric acid and the decomposition of some functional groups in this stage.

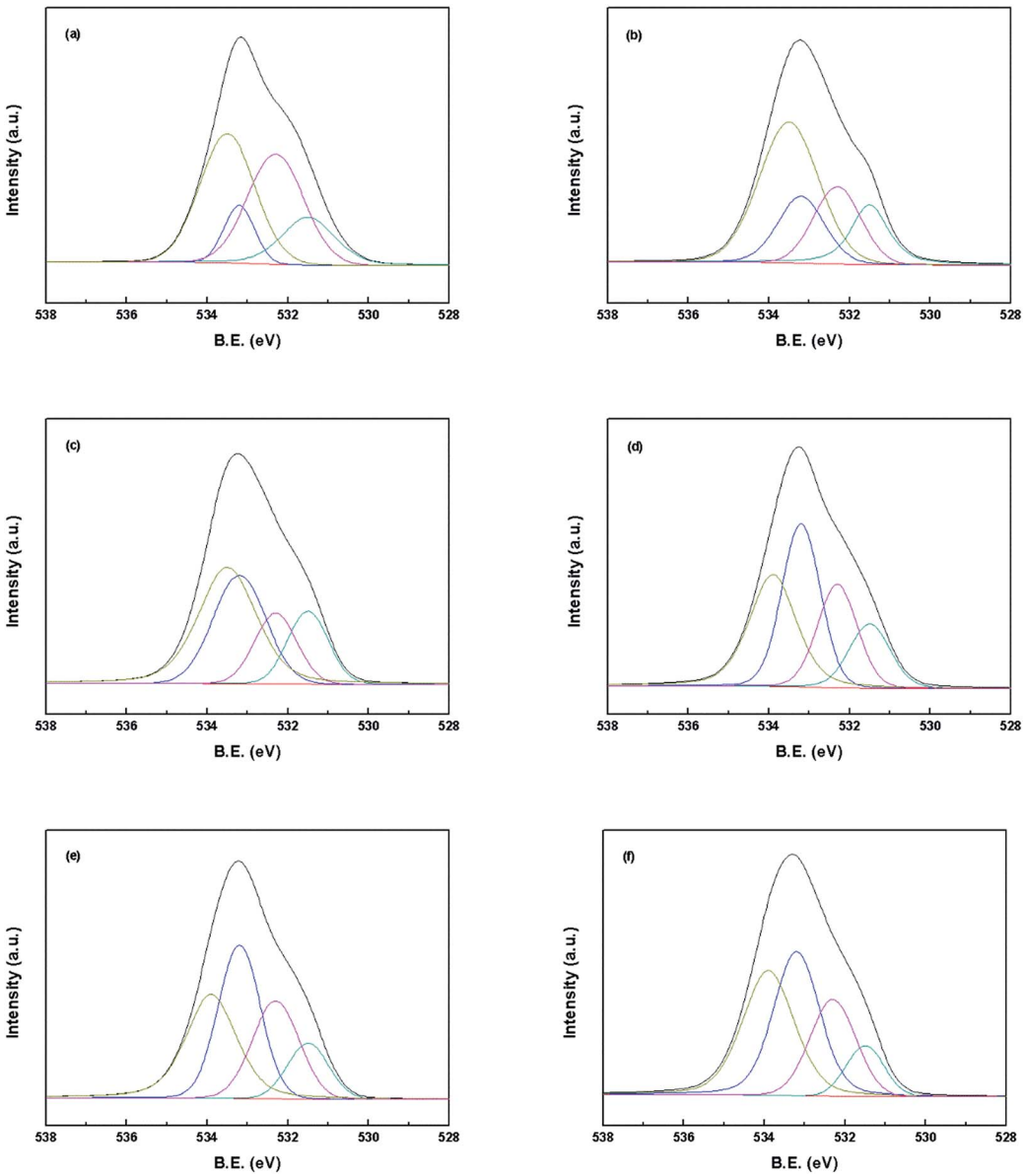

Fig. 9 XPS spectra of O1s peak of (a) PBTRHR and the samples (b–f) activated at 300, 400, 500, 600 and 700 °C.

Table 5 Relative content of the surface functional groups determined by O 1s spectra from XPS of (a) PBTRHR and (b–f) the samples activated at 300, 400, 500, 600 and 700 °C

Samples	Peak 1	Peak 2	Peak 3	Peak 4
(a)	15.9	34.5	9.8	39.8
(b)	15.5	19.8	17.7	47.0
(c)	15.4	15.4	29.4	39.8
(d)	14.3	21.7	32.9	31.1
(e)	11.7	23.4	33.5	31.4
(f)	9.2	23.8	35.1	31.9

From 400 to 700 °C, $H_{n+2}P_nO_{3n+1}$ should dehydrate and transform into P_4O_{10}, which presents various crystalline polymorphs and a vitreous modification, two such polymorphs melt between 500 and 600 °C.[42] P_4O_{10} which behaved as an oxidant reacted with carbon, forming new pores, widening the existing pores and producing CO_2. The phosphorus compound product of the reaction between P_4O_{10} and carbon was not phosphorus from the XPS of P 2p. It might be P_4O_6 according to O 1s and P 2p. The following reactions might occur:

$$H_{n+2}P_nO_{3n+1} \rightarrow P_4O_{10} + H_2O \quad (4)$$

$$P_4O_{10} + C \rightarrow P_4O_6 + CO_2 \quad (5)$$

The content of peak 1 decreased obviously from Table 5. It is mainly due to reduction of P_4O_{10} to P_4O_6, leading to the decrease of the content of P=O. The release of H_2O and CO_2 in this temperature range could be confirmed in TPD-MS. A little amount of CO decomposed from functional groups also existed in this stage.

From 700 to 800 °C, P_4O_{10} and/or P_4O_6 might react with CH_x in the substrate, generating PH_3 which could be detected in TPD-MS. The following reaction might occur:

$$P_4O_{10}/P_4O_6 + CH_x \rightarrow PH_3 + CO_2/CO \quad (6)$$

The amount of CO_2 and CO generated in this temperature range showed sharp increase. Moreover, the reaction between CO_2 and carbon to produce CO might exist at the same time. A. M. Puziy *et al.* found that elemental phosphorus was observed in the matrix of polymer-based carbon at the temperature as high as 1000 °C.[38] M. Myglovets *et al.* who take high-molecular-weight softwood sodium lignosulfonate as precursor pointed out that volatile phosphorus compounds might be formed by the following reactions above 750 °C:[43]

$$4H_3PO_4 + 10C \rightarrow P_4 + 10CO + 6H_2O$$

$$4H_3PO_4 + 10C \rightarrow P_4O_{10} + 6H_2O$$

$$P_4O_{10} + 10C \rightarrow P_4 + 10CO$$

The hydrogen elemental composition of BTRHR was low in our study, however, PH_3 still generated above 700 °C. The variation of phosphorus differed from these studies. This might be due to the difference between the precursors.

In our study, the activation process was divided in three temperature zones according to TGA-DTG results: the release of absorbed water and dehydration of H_3PO_4, the release of CO_2 and CO from the decomposition of functional groups from 100 to 400 °C; the release of H_2O dehydrated from H_3PO_4, the release of CO from the decomposition of functional groups, and CO_2 decomposed from the reaction and functional groups in the temperature range of 400–700 °C; PH_3 generated from the reaction, the release of CO_2 and CO generated from the reactions and the decomposition of functional groups from 700 to 800 °C. Above all, phosphoric acid played an important role in the activation process: (i) phosphoric acid seemed to be able to function as an acid catalyst in promoting bond cleavage reactions and the formation of crosslinks *via* such processes as cyclization and condensation; (ii) phosphoric acid acted as an oxidant after dehydration; and (iii) phosphoric acid connected with the substrate entering AC through C–O–P bond.

4. Conclusions

A series of AC samples were prepared from RHR by base treatment and chemical activation process in this study. The base treatment could remove ash and improve the surface area and pore volume. Chemical activation played an important role in increasing the surface area and pore volume. The valence state of phosphorus changed from +5 to −3 during the chemical activation process with H_3PO_4 from 100 to 800 °C. The reaction processes is quite complicated. The best results in terms of surface area (1016 $m^2\ g^{-1}$) was observed for a BTRHR/H_3PO_4 mass ratio of 1 : 2, an activation temperature of 500 °C and an activation time of 1 h.

Acknowledgements

This research was financially supported by the National High Technology Research and Development Program (863 program 2012 AA 051803) of China and the characterization of the samples from Analytic and Testing Center of Sichuan University was highly acknowledged.

Notes and references

1 X. Song, Y. Zhang and C. Chang, *Ind. Eng. Chem. Res.*, 2012, **51**, 15075–15081.
2 W. Shi, J. Jia, Y. Gao and Y. Zhao, *Bioresour. Technol.*, 2013, **146**, 355–362.
3 J. Alvarez, G. Lopez, M. Amutio, J. Bilbao and M. Olazar, *Fuel*, 2014, **128**, 162–169.
4 X. Zhang, Y. Li, G. Li and C. Hu, *RSC Adv.*, 2015, **5**, 4984–4992.
5 Y. Liu, Y. Guo, Y. Zhu, D. An, W. Gao, Z. Wang, Y. Ma and Z. Wang, *J. Hazard. Mater.*, 2011, **186**, 1314–1319.
6 Y. Liu, Y. Guo, W. Gao, Z. Wang, Y. Ma and Z. Wang, *J. Cleaner Prod.*, 2012, **32**, 204–209.
7 T. H. Liou and S. J. Wu, *J. Hazard. Mater.*, 2009, **171**, 693–703.
8 O. A. Ioannidou, A. A. Zabaniotou, G. G. Stavropoulos, M. A. Islam and T. A. Albanis, *Chemosphere*, 2010, **80**, 1328–1336.
9 M. Molina-Sabio and F. Rodríguez-Reinoso, *Colloids Surf., A*, 2004, **241**, 15–25.
10 N. V. Sych, S. I. Trofymenko, O. I. Poddubnaya, M. M. Tsyba, V. I. Sapsay, D. O. Klymchuk and A. M. Puziy, *Appl. Surf. Sci.*, 2012, **261**, 75–82.
11 V. Fierro, G. Muñiz, A. H. Basta, H. El-Saied and A. Celzard, *J. Hazard. Mater.*, 2010, **181**, 27–34.
12 M. Al Bahri, L. Calvo, M. A. Gilarranz and J. J. Rodriguez, *Chem. Eng. J.*, 2012, **203**, 348–356.
13 L. Lin, S. R. Zhai, Z. Y. Xiao, Y. Song, Q. D. An and X. W. Song, *Bioresour. Technol.*, 2013, **136**, 437–443.
14 C. Michailof, G. G. Stavropoulos and C. Panayiotou, *Bioresour. Technol.*, 2008, **99**, 6400–6408.
15 M. Jagtoyen and F. Derbyshire, *Carbon*, 1998, **36**, 1085–1097.
16 J. M. Rosas, R. Ruiz-Rosas, J. Rodríguez-Mirasol and T. Cordero, *Carbon*, 2012, **50**, 1523–1537.
17 Q. Lu, X.-L. Yang and X.-F. Zhu, *J. Anal. Appl. Pyrolysis*, 2008, **82**, 191–198.
18 I. Othman Ali, A. M. Hassan, S. M. Shaaban and K. S. Soliman, *Sep. Purif. Technol.*, 2011, **83**, 38–44.
19 L. J. Kennedy, J. J. Vijaya and G. Sekaran, *Ind. Eng. Chem. Res.*, 2004, **43**, 1832–1838.
20 P. Barpanda, G. Fanchini and G. G. Amatucci, *Carbon*, 2011, **49**, 2538–2548.
21 Y. Guo and D. A. Rockstraw, *Microporous Mesoporous Mater.*, 2007, **100**, 12–19.
22 J. Zhang, H. Fu, X. Lv, J. Tang and X. Xu, *Biomass Bioenergy*, 2011, **35**, 464–472.
23 Y. Juan and Q. Ke-Qiang, *Environ. Sci. Technol.*, 2009, **43**, 3385–3390.
24 T.-H. Liou, *Carbon*, 2004, **42**, 785–794.

25 A. M. Puziy, O. I. Poddubnaya, A. Martıínez-Alonso, F. Suárez-García and J. M. D. Tascón, *Carbon*, 2002, **40**, 1493–1505.
26 Y. Chen, S. R. Zhai, N. Liu, Y. Song, Q. D. An and X. W. Song, *Bioresour. Technol.*, 2013, **144**, 401–409.
27 R. Pierotti and J. Rouquerol, *Pure Appl. Chem.*, 1985, **57**, 603–619.
28 H. Teng, T.-S. Yeh and L.-Y. Hsu, *Carbon*, 1998, **36**, 1387–1395.
29 M. Molina-Sabio, F. Rodriguez-Reinoso, F. Caturla and M. Selles, *Carbon*, 1995, **33**, 1105–1113.
30 S. Timur, I. C. Kantarli, E. Ikizoglu and J. Yanik, *Energy Fuels*, 2006, **20**, 2636–2641.
31 Y. Li, X. Ding, Y. Guo, C. Rong, L. Wang, Y. Qu, X. Ma and Z. Wang, *J. Hazard. Mater.*, 2011, **186**, 2151–2156.
32 D. Prahas, Y. Kartika, N. Indraswati and S. Ismadji, *Chem. Eng. J.*, 2008, **140**, 32–42.
33 M. Zhi, F. Yang, F. Meng, M. Li, A. Manivannan and N. Wu, *ACS Sustainable Chem. Eng.*, 2014, **2**, 1592–1598.
34 L. Ding, B. Zou, L. Shen, C. Zhao, Z. Wang, Y. Guo, X. Wang and Y. Liu, *Colloids Surf., A*, 2014, **446**, 90–96.
35 T. Durkić, A. Perić, M. Laušević, A. Dekanski, O. Nešković, M. Veljković and Z. Laušević, *Carbon*, 1997, **35**, 1567–1572.
36 M. O. Guerrero-Pérez, M. J. Valero-Romero, S. Hernández, J. M. L. Nieto, J. Rodríguez-Mirasol and T. Cordero, *Catal. Today*, 2012, **195**, 155–161.
37 P. Y. Shih, S. W. Yung and T. S. Chin, *J. Non-Cryst. Solids*, 1999, **244**, 211–222.
38 A. M. Puziy, O. I. Poddubnaya, R. P. Socha, J. Gurgul and M. Wisniewski, *Carbon*, 2008, **46**, 2113–2123.
39 A. Castro-Muniz, F. Suarez-Garcia, A. Martinez-Alonso and J. M. Tascon, *J. Colloid Interface Sci.*, 2011, **361**, 307–315.
40 M. Zhi, S. Liu, Z. Hong and N. Wu, *RSC Adv.*, 2014, **4**, 43619–43623.
41 M. A. Nahil and P. T. Williams, *Biomass Bioenergy*, 2012, **37**, 142–149.
42 M. Olivares-Marín, C. Fernández-González, A. Macías-García and V. Gómez-Serrano, *Carbon*, 2006, **44**, 2347–2350.
43 M. Myglovets, O. I. Poddubnaya, O. Sevastyanova, M. E. Lindström, B. Gawdzik, M. Sobiesiak, M. M. Tsyba, V. I. Sapsay, D. O. Klymchuk and A. M. Puziy, *Carbon*, 2014, **80**, 771–783.

